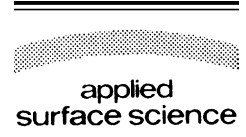


Available online at www.sciencedirect.com

SCIENCE @ DIRECT®

Applied Surface Science xxx (2006) xxx–xxx

www.elsevier.com/locate/apsusc

Superior refractive index tailoring properties in composite ZrO₂/SiO₂ thin film systems achieved through reactive electron beam codeposition process

N.K. Sahoo*, S. Thakur, R.B. Tokas

Spectroscopy Division, Bhabha Atomic Research Centre, Trombay, Mumbai 400085, India

Received 21 November 2005; accepted 21 December 2005

Abstract

Composite optical thin-film materials have received a significant amount of interest in order to relieve the material constraints on refractive indices as well as reducing the number of layers required in optical coating design. Amongst others binary zirconia–silica composite thin films have attracted considerable attentions due to their several favorable opto-mechanical properties. In the present studies such a composite system under certain compositional mixings displayed both refractive index and band gap supremacy over pure zirconia films violating the most popular Moss rule. This unexpected evolution has several practical applications one of which can be directly employed in extending the range of tunability of the refractive index. Besides, the probing of such a novel evolution through the analysis of ellipsometric refractive index modeling and morphological correlation functions has revealed several novel as well as superior microstructural properties in the composite thin film systems. All these characterization and analysis techniques distinctly indicate a strong interrelation between the microstructural ordering and superior optical properties of the present zirconia–silica codeposited composites.

© 2006 Elsevier B.V. All rights reserved.

PACS: 42.79.Wc; 78.66.–w; 78.20.Ci; 61.16.Ch; 51.70.+f; 52.70.Kz

Keywords: Optical coatings; Optical thin films; Codeposition; Electron beam evaporation; Ellipsometry; Atomic force microscopy; Composite films; Correlation functions

1. Introduction

The need for advanced optical materials endowed with enhanced properties has progressively focused on composite systems which can involve complex stoichiometry and/or microstructures [1–3]. There are two main advantages that can be derived from a binary composite system. The first and foremost is the tailoring of the material properties between the two participating components and the other being the superior microstructure [3,4]. Besides, several other novel evolutionary properties may sometime begin to appear which not only contribute to the pleasant surprise but also further extend the usefulness of the composite material [5,6]. The presently studied zirconia–silica (ZrO₂/SiO₂) composite system has depicted several such novel properties which have distinct

advantages both with respect to the tunability in the refractive index as well as the superior microstructure that controls the band gap favorably. It was distinctly noticed that by admixing silica in ZrO₂, under certain compositional ratios the optical properties such as polarizability (or refractive index), energy gap, etc., are dominantly influenced by the microstructure than the stoichiometry. Such an influence leads to situation where certain zirconia–silica composite films have displayed superior refractive index values than that of the pure zirconia. Besides, these films also depicted superior band gap values violating the most popular Moss semi-empirical rule [7–10].

It can be mentioned here that the interrelation between energy gap (E_g) and high frequency refractive index (n_∞) in semiconductors and dielectrics is manifested by an inverse law which popularly known as Moss rule [7–15]. Mathematically it is given by,

$$n_\infty^4 E_g = \text{constant} \quad (1)$$

* Corresponding author. Fax: +91 22 5505151.

E-mail address: nksahoo@apsara.barc.ernet.in (N.K. Sahoo).

This semi-empirical relationship is based on the fundamental principle that in a dielectric medium all energy levels are scaled down by a factor of square of the dielectric constant (ϵ^2) or fourth power of the refractive index (n^4). Such a rule is obeyed by most semiconductors with a few rare violations during which the materials display several interesting parametric and microstructural evolutions [16,17]. For example, in gain-guided semiconductor lasers in the junction plane and also in the plane perpendicular to the junction, a reduction in band gap involves a refractive index decrease (e.g., active InAs on GaSb substrate) [16].

The present results are based on some specific composites involving $\text{ZrO}_2/\text{SiO}_2$ thin film systems that have displayed superior refractive index and energy gaps simultaneously violating the semi-empirical Moss rule. Besides these superior qualities can be utilized effectively in extending the range of refractive index tailoring or tuning. In the past, zirconia–silica composite system has attracted the attentions of several thin film researchers both application point of view as well as the aspects related to probing of its microstructural evolutions [18,19]. Some researchers have very distinctly noticed a microstructural transition under the admixture of certain volume fractions of silica films to zirconia without any suitable explanation for such an unexpected evolution [20]. A few research studies have proposed a theory of grain structure densification through a volumetric analysis of such composite films [21]. Some experimentalists also have postulated the theory of void structure reduction and grain structure transition under the influence of glassy silica component films [22–24]. In spite of these attempts, so far there is no very authentic explanation for such exceptional and superior optical property in composite films supported by the advanced characterization results and evidences. Under our present experimental data analyses we, however, noticed a prominent microstructural ordering that led to superior optical qualities as well as violation of Moss rule in such composite films. Besides, morphological measurement results through atomic force microscopy revealed a grain structure densification as well as void structure reduction in these composite thin films. The morphological derived functions such autocorrelation and height–height correlation functions and their analyses distinctly supported such phenomena of better microstructural ordering [25–28].

2. Experimental details

Under the present investigation, we have carried out some systematic experiments and analysis of codeposited thin films of $\text{ZrO}_2/\text{SiO}_2$ system using phase modulated ellipsometry, spectrophotometry and multimode scanning probe microscope (SPM) techniques. However, as mentioned above, this research paper predominantly presents the results of ellipsometric and SPM measurements and analyses. The samples were deposited in a fully automatic thin film vacuum system “VERA-902” by adopting the reactive electron beam deposition technique. The depositions of the films were carried out using two 8 KW VTD electron beam guns with sweep and automatic emission

controls. The film materials for SiO_2 and ZrO_2 were chosen from Cerac’s batch number “S-1060” (purity 99.99%) and “Z-1056” (purity 99.995%), respectively. The substrate temperature was maintained at 70 °C for the deposited films. The total pressure inside the chamber during the deposition process was maintained at 1×10^{-4} mbar through MKS mass flow controllers. The constituents of the gases present during the deposition were analyzed by a residual gas analyzer (RGA) model; Pfeiffer’s Prisma-200. The film thicknesses were monitored both using the Leybold’s OMS-2000 optical thickness monitor (OTM) as well as Inficon’s XTC/2 quartz crystal monitors (QCM). The individual rates of depositions were very accurately monitored as well as controlled in automatic feed-back mode as per the requirements of the codeposition process. The proportional, integration and differential (PID) parameters of the thickness as well as process control systems were judiciously optimized in order to avoid unwanted rate fluctuations during codeposition processes. By such appropriate and accurate rate controls, it was possible to obtain $\text{ZrO}_2/\text{SiO}_2$ codeposited composite films with the desired compositions in the ranges of 10–90%. The entire deposition process parameters such as substrate temperature, optical thicknesses, rates of deposition, total reacting gas pressure were monitored and controlled by a Siemen’s industrial programmable logic controller (PLC) with appropriate front-end software. The codeposited film optical thicknesses were decided to remain six to eight quarter-wave ($\lambda/4$) at a wavelength of 600 nm, in order to obtain appropriate numbers of interference fringes for spectrophotometric as well as ellipsometric analysis techniques.

For ellipsometric studies, Jobin Yvon’s phase modulated spectroscopic ellipsometer model UVISEL has been employed to analyze the growth dependent spectral optical properties. As described above Tauc–Lorentz (TL) formulation has been adopted to probe the codeposited films for their refractive index profile using a discrete multilayer approach. The spectral refractive indices are further analyzed using effective single oscillator model in order to probe deep in to the ordered microstructures. For AFM characterization, NT-MDT’s solver P-47H multimode ambient-based scanning probe system has been utilized. The cantilever used was a Si_3N_4 with typical spring constant of 0.6 N/m and resonant frequency of 75 kHz. We have adopted the contact mode operation without any image filtering technique for the topographic measurements. For Fourier analysis, the built-in FFT module of the control software “NOVA-SPM” was employed to generate the mappings. Similarly, for autocorrelation function (ACF) analysis the built in features are employed to compute both the 2D and 3D ACF parameters. In order to have the consistency in the experimental results, the same cantilever was used for all the topographic measurements. All the codeposited films were spectrally measured for their reflectance as well as transmittance characteristics using Shimadzu UV3101PC spectrophotometer system equipped with an integrating sphere accessory. The results of various characterization techniques as well as model parameterization have been presented in the subsequent sections.

3. Tauc–Lorentz model and ZrO₂/SiO₂ composite structures

The Tauc–Lorentz model is a powerful tool with which it has now become extremely convenient to parameterize interband absorption above the band edge [29]. Although this model was derived for amorphous semiconductor, it can be conveniently applied to polycrystalline and nanocrystalline thin films as well [30]. For example to model the dielectric functions in HfO₂ films, the Tauc–Lorentz dispersion was successfully adopted for the amorphous and polycrystalline films by Cho et al. [31]. The application of this model for the parameterization of the optical absorption of TiO₂, Ta₂O₅, HfO₂, Al₂O₃ and LaF₃ polycrystalline thin-film materials has been described by von Blanckenhagen et al. [32]. In order to appreciate the importance of such an empirical approach, a brief description of the parameters involved in the modeling process is highly beneficial.

Essentially, the Tauc–Lorentz model supplies an expression for the imaginary part, ε_2 , of the dielectric function if only a single transition is considered. We obtain the model by multiplying the Tauc expression for ε_2 near the band edge by the imaginary part of the complex dielectric function of a single Lorentz oscillator [29,32]:

$$\varepsilon_2 = \frac{AE_0\Gamma(E - E_g)^2}{(E^2 - E_0^2)^2 + \Gamma^2 E^2} \frac{1}{E}, \quad E > E_g \quad (2)$$

$$\varepsilon_2 = 0, \quad E \leq E_g \quad (3)$$

where E_g is the band gap, E_0 the peak transition energy, Γ a broadening parameter and the factor A which represents the optical transition matrix elements. All these parameters have very special significances and contribute immensely to the dielectric function. For instance, the broadening parameter Γ is related to the degree of disorder in the material. Similarly, the parameter A which is proportional to the height of ε_2 , related to the film density. The real part of the dielectric function ε_1 is obtained by the Kramers–Kronig integration of ε_2 [29]:

$$\varepsilon_1 = \varepsilon_\infty + \frac{2}{\pi} P \int_{E_g}^{\infty} \frac{\xi \varepsilon_2(\xi)}{\xi^2 - E^2} d\xi \quad (4)$$

where ε_∞ represents the contribution of the optical transitions at higher energies and appears as an additional fitting parameter. In the present work this formulation has been adopted to model the experimental ellipsometric functional parameters in order to derive the desired spectral refractive indices and band gaps for the composite films.

4. Analysis by single-effective oscillator model

Results of refractive index dispersion below the interband absorption edge correspond to the fundamental electronic excitation spectrum may assist very important discussion on the dielectric constant of the material. Wemple and DiDomenico have analyzed more than 100 widely different solids and liquids using a single-effective oscillator model [33]. Based upon the

validity of Kramers–Kronig relationship, equations for ε_r and ε_i were given by them. Equation for the real part takes the form:

$$\varepsilon_r^2(E) = 1 + \frac{F}{E_0^2 - E^2} \quad (5)$$

where, the two parameters E_0 and F have straightforward relations to the electric dipole strength and the corresponding transition frequencies of all oscillators. The parameters used in this expression have fundamental as well as physical significances. By a special combination of parameters, Wemple and DiDomenico [33] defined a microstructural variable E_d as:

$$E_d = \frac{F}{E_0} \quad (6)$$

Combination of Eqs. (4) and (5), neglecting values of k in the transparent region gives:

$$\varepsilon_r(E) = n^2(E) = 1 + \frac{E_d E_0}{E_0^2 - E^2} \quad (7)$$

Values of the parameters E_0 and E_d were estimated by plotting $(n^2 - 1)^{-1}$ versus E^2 and fitting the relation to a straight line. These two parameters of the model are: the dispersion energy $E_d = \hbar B/E_0^2$ that measures the average strength of interband optical transitions and is associated with the changes in the structural order of the material and the effective oscillation energy E_0 which can be directly correlated with the optical band gap by an empirical formula. The increase of the dispersion energy value (E_d) is usually associated with evolution of the thin film microstructure to a more ordered phase [34]. On the basis of the single-effective oscillator model however, E_0 and E_d are connected to ε_i and the M_{-1} and M_{-3} moments of the $\varepsilon(E)$ optical spectrum, through the relations:

$$E_0^2 = \frac{M_{-1}}{M_{-3}} \quad (8)$$

$$E_d^2 = \frac{M_{-1}^3}{M_{-3}} \quad (9)$$

where the r th moment of the optical spectrum is given by:

$$M_r = \frac{2}{\pi} \int_{E_t}^{\infty} E^r \varepsilon_i(E) dE \quad (10)$$

and E_t is the absorption threshold energy. The refractive index is related to the imaginary part of complex electronic dielectric constant $\varepsilon(\omega) = \varepsilon_1(\omega) + \varepsilon_2(\omega)$, where ω is the photon frequency. Either the real part or the imaginary part contains all the information about the electronic excitation spectrum of the material, since one of them is connected to the other one by the Kramers–Kronig relation [35].

The oscillator energy E_0 is independent of the scale of ε_2 and is subsequently an “average” energy gap, where as E_d depends on the scale of ε_2 , and thus serves as an interband strength parameter. Since the -1 and -3 moments are involved in computation of E_0 and E_d , the ε_2 spectrum is weighted most heavily near the interband absorption threshold. It is further added that the oscillator energy E_0 is very similar to the energy

parameter used by Penn, being a measure of the energy difference between the “centers of gravity” of the valence and conduction bands [36]. This value is different from the optical gap which probes the optical properties near the band edges of the material.

5. Analysis by morphological correlation functions

Although, at the first sight, thin film morphology is appeared to be random, a close analysis reveals volumes of correlated properties. The best way the thin film morphology can be probed is by analyzing its ACF as well as height–height correlation function (HHCF) [37]. Spatial autocorrelation is, conceptually as well as empirically, the two-dimensional equivalent of redundancy. It measures the extent, to which the occurrence of an event in a designated unit constrains, or makes more probable, the occurrence of an event in its neighboring unit. In other words, the autocorrelation function can be used to detect non-randomness in surface data as well as to identify an appropriate space or time series model if the data are not random. Within the AFM measurements we usually evaluate the one-dimensional autocorrelation function determined only from the height profiles

($z_{n+m,l}$ and $z_{n,l}$) in the fast scanning axis which can be evaluated from the discrete ($N \times M$) AFM data values as [38],

$$A_x(\tau_x) = \frac{1}{N(M-m)} \sum_{l=1}^N \sum_{n=1}^{M-m} z_{n+m,l} z_{n,l} \quad (11)$$

In the present studies several codeposited thin films of zirconia–silica systems have been analyzed for their morphologies as well as autocorrelation functions using the data and information acquired through the Solver P-47H atomic force microscope (AFM) measurements. The autocorrelation functions of pure film and the composites have shown very different trends in their evolution. However, in most of the codeposited films, such functions can be fitted well with the appropriate realistic Gaussian models.

Height–height correlation function is also very intimately associated with the autocorrelation and very prominently represents the grain structures in thin film morphology. Mathematically, it is given by [39],

$$H_x(r_x) = \frac{1}{N(M-m)} \sum_{l=1}^N \sum_{n=1}^{M-m} (z_{n+m,l} - z_{n,l})^2 \quad (12)$$

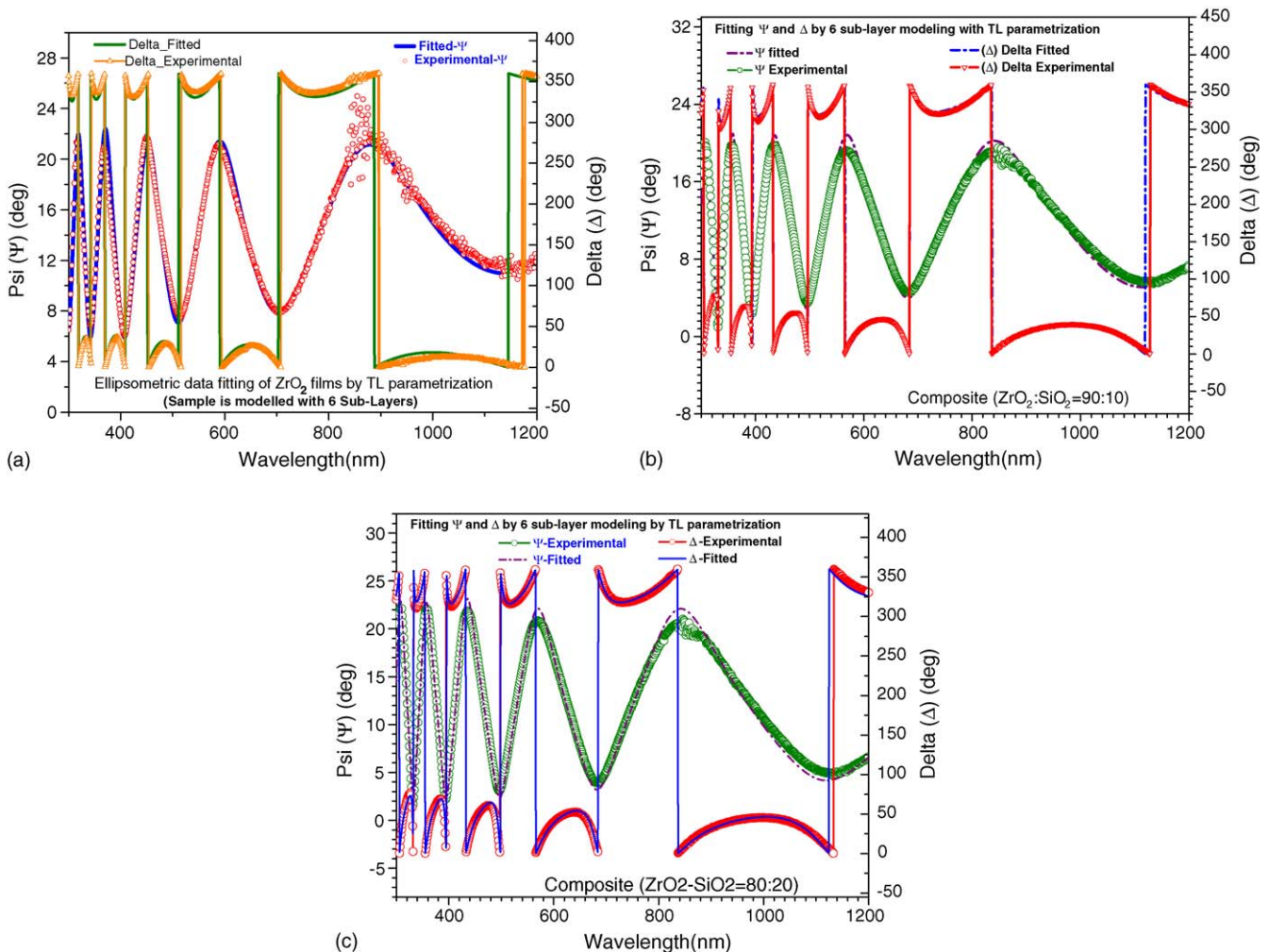


Fig. 1. Ellipsometric (Ψ , Δ) modeling of (a) pure zirconia film, composite gadolinia–silica with (b) 90/10 and (c) 80/20 mixing ratios carried out using Tauc–Lorentz parameterization. In order to account for the growth dependent inhomogeneity appropriate multilayer approaches have been adopted.

In order to get insight into the dynamic behavior and the growth processes related evolution of morphology in the pure and composite films, we calculated the height–height correlation function $H(r)$ based on the AFM data. Like most thin film experiments, here also it is expected that for each film, $\log H(r)$ should increase linearly with $\log r$ for small distance r , depicting a power-law behavior represented by, $H(r) \propto r^{2\alpha}$ and then leading to saturation for large r . At the initial regime of the correlation function there exist variant slopes representing different microstructural evolutions in composite and pure films. With this concept, we have tried to fit the height–height correlation function with the self-affine properties using the relationship [40],

$$H(r) = 2w^2 \left[1 - \exp \left(- \left(\frac{r}{\xi} \right)^{2\alpha} \right) \right] \quad (13)$$

where w is related to the interface width, α the roughness exponent and ξ is the lateral correlation length. All these parameters have very special significances with the respect to the qualitative as well as quantitative behavior of the surface morphology. For instance, α , the roughness exponent, signifies the how “wiggly” the local slope is. It is also an indicative of the “jaggedness” of the topography as well as signifies the relative contribution of high frequency fluctuations to the roughness. Its value is directly correlated with “*Herst*” exponent that define the fractal dimension of the surfaces. On the very short length scale, this parameter α is connected with the fractal dimension as “ $D = 3 - \alpha$ ” [41]. The lateral correlation length, ξ , describes the largest distance in which the height is still correlated. It is to be further noted that, ξ provides a length scale which distinguishes the short-range and long-range behaviors of the rough surface. The interface width, w , is a measure of the surface height fluctuation, i.e., it signifies the RMS fluctuation about the mean height. So, close looks and detailed analysis of these parameters w , α and ξ reveal several factors that represent the

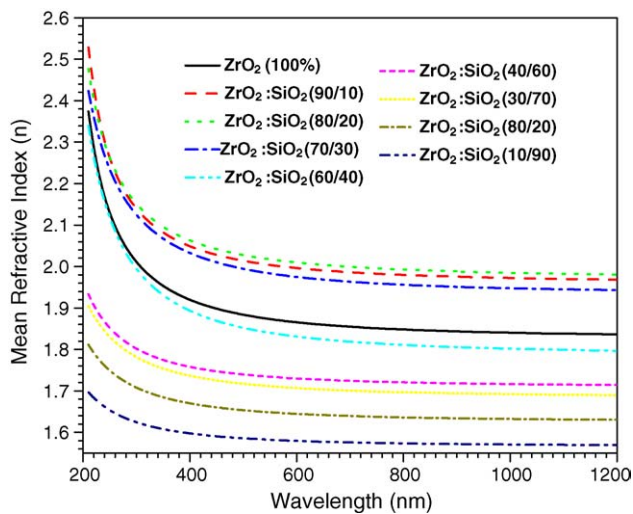


Fig. 2. Spectral refractive index profiles of composite zirconia–silica films in the mixing ratios from 90/10 to 10/90. It can be seen in this plot that the optical properties and compositional mixings do not obey a linear interrelation.

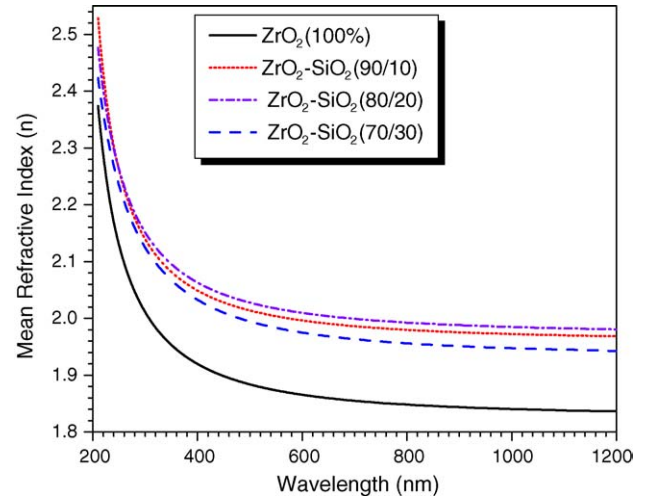


Fig. 3. Spectral refractive index profiles of pure zirconia and composite films with silica component 10% to 30%. These composite films have displayed much superior values in their optical properties.

interrelation between the morphology and microstructure of the codeposited thin films.

6. Results and discussions

Experimental ellipsometric parameters (Ψ , Δ) and their fittings with Tauc–Lorentz model for some of the pure zirconia and composite zirconia–silica films are presented in Fig. 1 (a–c). It is worth mentioning that the growth dependent refractive index of all most all the pure and composite films depicted certain non-linear inhomogeneous behavior. Modeling and analysis of such inhomogeneous profiles is a very challenging task and one has to adopt judiciously chosen multilayer formalisms. Under this technique each layer is split into a finite number of sub-layers with different dispersive optical and microstructural parameters as per TL model in order

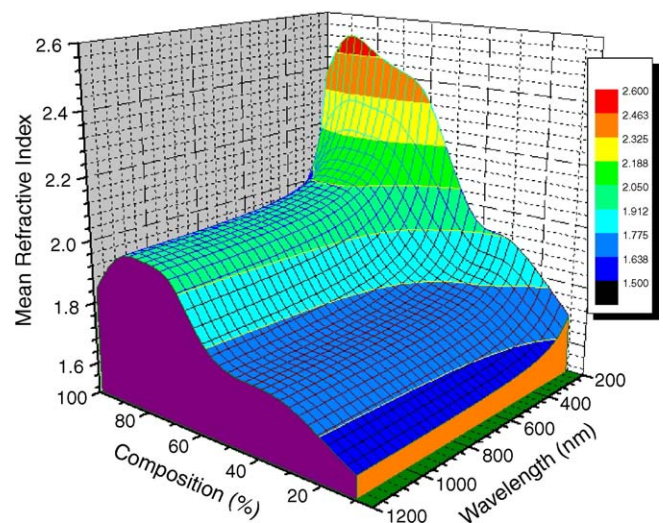


Fig. 4. Three-dimensional (3D) fit to the spectral refractive index profiles of the composite zirconia–silica thin films. It can be distinctly seen here the refractive index supremacies of composite films with certain mixing ratios.

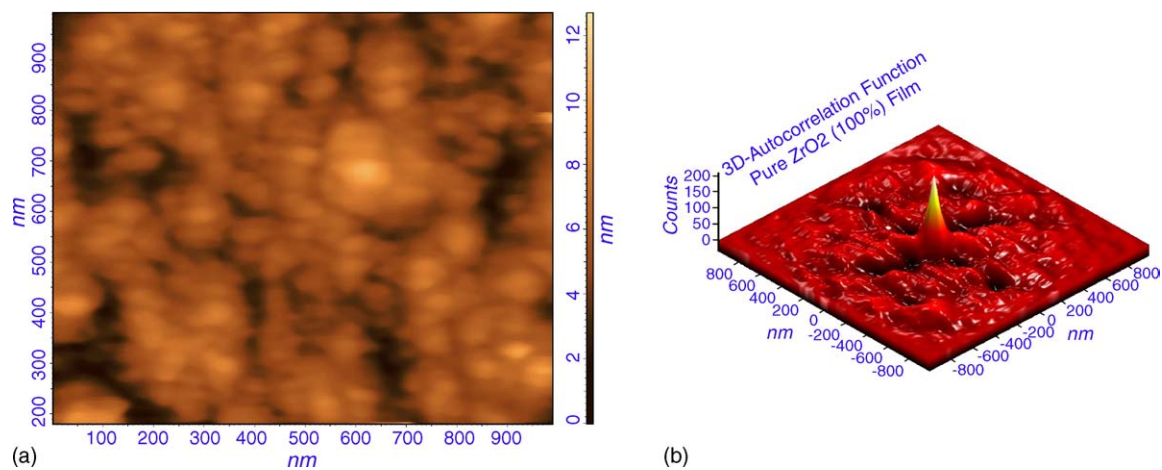


Fig. 5. (a) Morphology and (b) derived 3D autocorrelation function for pure zirconia (100% ZrO_2) film. It can be seen here that the pure zirconia film has more voids with dominant mounds or superstructures.

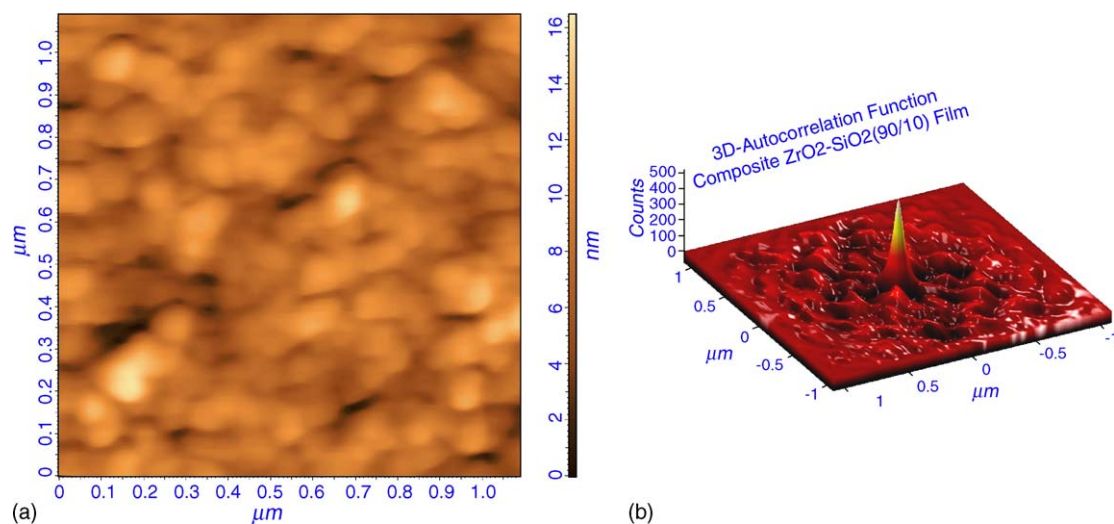


Fig. 6. (a) Morphology and (b) derived 3D autocorrelation function for pure zirconia-silica (ZrO_2-SiO_2 (90/10)) film. Morphology displayed a more dense grain structure with large distributed features in the 3D autocorrelation analysis.

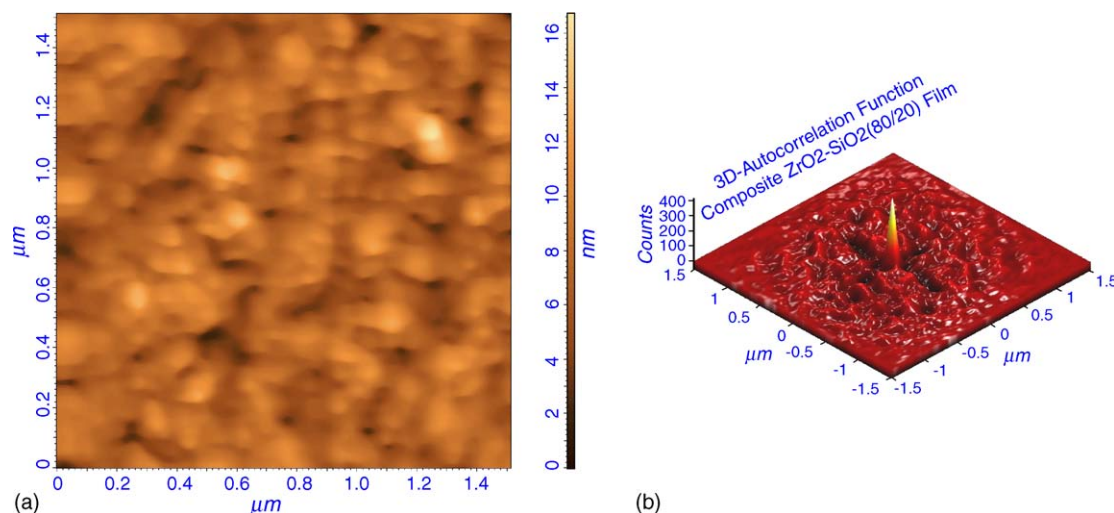


Fig. 7. (a) Morphology and (b) derived 3D autocorrelation function for pure zirconia-silica (ZrO_2-SiO_2 (80/20)) film. Morphology displayed a still better dense grain structure with relatively small and uniformly distributed features in the 3D autocorrelation figure.

to account for the mean experimental spectroscopic ellipsometric results. The mean or effective optical parameters have been computed by taking account of such multilayer substructures as well as the weighted mean of the growth-dependent non-linear microstructural parameters. The goodness in ellipsometric fits presented in Fig. 1(a–c) distinctly supports such a multilayer analysis approach. Mean refractive index profiles for various composite films computed adopting such TL formalisms are depicted in Fig. 2. It can be noticed from this figure that films with a silica composition of 10–20% have demonstrated superior spectral profiles. Composite films which have such superior refractive index profiles with respect to pure zirconia film are specially presented in Fig. 3. A three dimensional fit to the spectral refractive index profiles distinctly indicating superior features are presented in Fig. 4. This figure has very prominently shown both wavelength as well as composition dependent evolutions of the refractive index profiles of the composite films. In order to probe this feature deep, we have analyzed their morphologies acquired through Solver P-47H atomic force microscope. The topographies and their derived 3D autocorrelation functions of the films that show distinct changes are presented in Figs. 5–7. It can be noticed from Fig. 5(a) that the pure zirconia films have displayed localized mounds or superstructures with a relative poor density in their grain distributions. The same results are also reflected in the 3D autocorrelation function depicted in Fig. 5(b). The morphologies in case of composite films with silica composition of 10–20% distinctly displayed a dense microstructure as depicted in Figs. 6(a) and 7(a) supporting the superior values of the spectral refractive indices. The 3D autocorrelation functions for these morphologies presented in Figs. 6(b) and 7(b) have displayed a more uniformly distributed features hinting towards some kind of self-affine type of characteristics. 2D autocorrelation functions of these films are presented in Fig. 8(a–c). It can be seen that autocorrelation counts are increased in the composite films with the highest

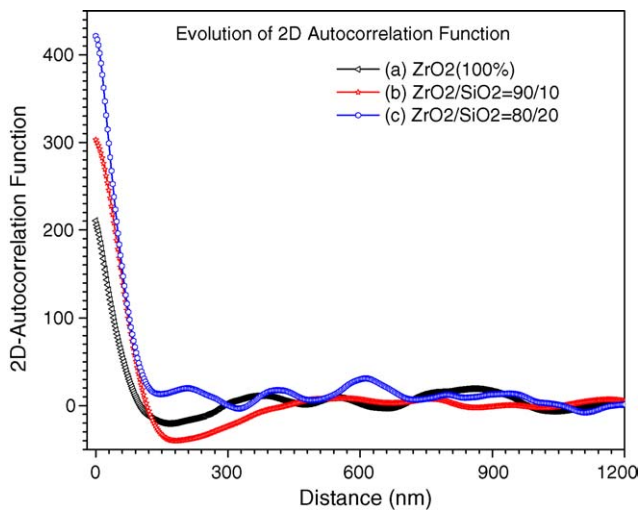


Fig. 8. Two-dimensional autocorrelation functional (ACF) analyses comparing the (a) pure and composite films with $\text{ZrO}_2/\text{SiO}_2$ mixing ratios of (b) 90/10 and (c) 80/20. Composite films have shown better correlation lengths implying improve structural ordering.

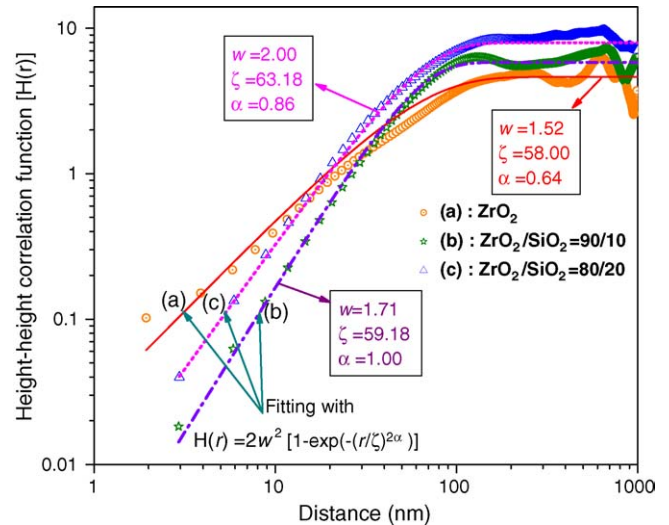


Fig. 9. Height–height correlation functional (HHCF) analyses of (a) pure and composite zirconia films with the mixing ratios of (b) 90/10 and (c) 80/20. The pure zirconia film has demonstrated a different slope in its HHCF function with respect to composite films. All the derived parameters like roughness exponent (α), correlation length (ξ) and interface width (w) have displayed superior values for the composite films.

value for the films with 80/20 ratio of $\text{ZrO}_2/\text{SiO}_2$ compositions. The height–height correlation functions of these films are presented in Fig. 9(a–c). In order to derive the microstructural correlation parameters each experimental HHCF function was fitted using the self-affine model given in Eq. (13). Numerical values of various fitted correlation variables are also presented in this figure. It can be seen here that the pure zirconia has demonstrated lowest values for the correlation length (ξ), the roughness exponent (α) and the interface width (w) parameters. This infers that the composite films have a more ordered structure with higher densities than that of the pure zirconia film. This aspect was also probed through the analysis of ellipsometric variables using TL formalisms. The two most important TL variables “A”, the density parameter and “ Γ ”, the disorder parameter, are presented in Fig. 10. It is to be

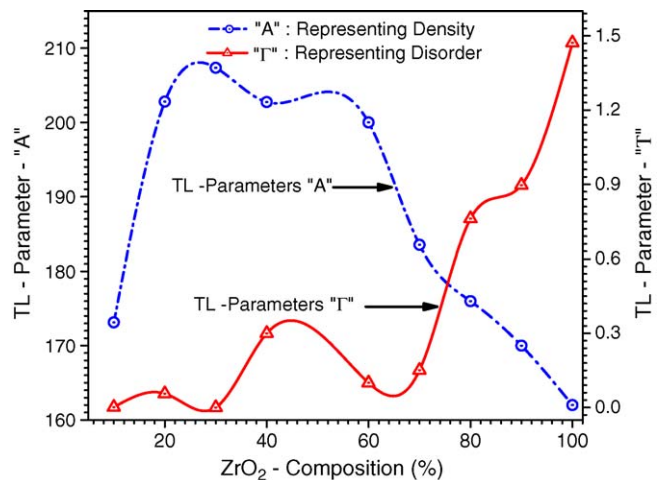


Fig. 10. Tauc–Lorentz parameters A and Γ representing density and disorder in thin films. It can be seen that composite films have displayed a relatively better density and lower values for the disorder parameter.

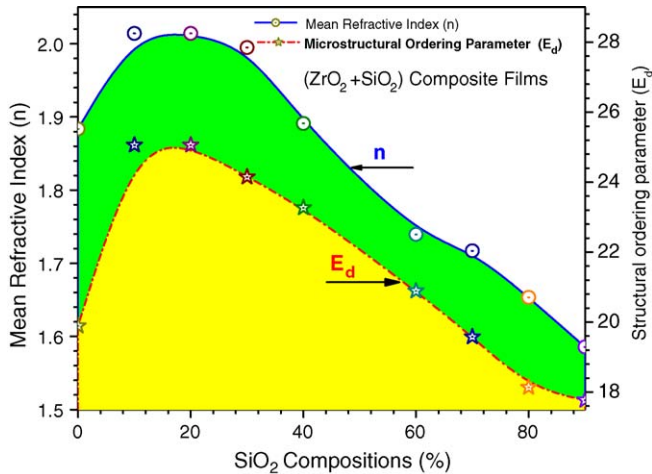


Fig. 11. Plot of refractive index (n) and order microstructure parameter (E_d) acquired through effective single oscillator modeling. It can be seen here that both these parameters have one-to-one correspondence implying a strong interrelation between the optical properties and the microstructure.

noticed here that the composite films have displayed both superior densities as well as ordered microstructure. These aspects are also probed with the help of effective single oscillator model. The evolution of refractive index (n) and structural ordering parameter (E_d) is presented in Fig. 11. It can be seen here that both these variables follow each other indicating that there is one to one correspondence between the evolutions in the refractive index and the order microstructure. The most interesting aspect noticed in the present experiment is the superior features of certain composite films over the pure zirconia film. In Fig. 12 the results related to the refractive index and band gap evolutions are presented where the distinct violation of Moss rule can be noticed. Composite films with the presence of 10–20% silica component demonstrated much superior spectral refractive index as well as energy gap values. Such a condition can favorably be utilized in

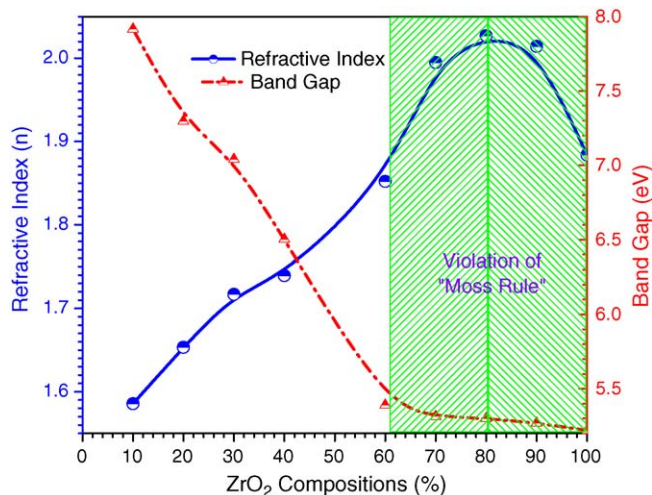


Fig. 12. Plots of refractive index and band gap over various compositions of the composite films. In shaded area, the composite films have depicted superior value in refractive indices and band gaps simultaneously violating the most popular semi-empirical Moss rule.

extending the refractive tuning limits to beyond the values of the two participating components.

7. Conclusions

The presently studied composite zirconia–silica thin films deposited through reactive electron beam codeposition process have demonstrated several interesting optical, microstructural and morphological evolutions. The optical and microstructural properties were probed using phase modulated spectroscopic ellipsometry and multi-mode scanning probe microscopy. Several analyses techniques including Tauc–Lorentz parameterization and effective single oscillator models have been employed to derive optical and microstructural parameter from the spectral Ψ and Δ measurements. The morphological parameters were modeled with autocorrelation and height–height correlation functions. In order to derive the microstructural variables and parameters the height–height correlation functions of pure as well as composite zirconia films were analyzed using a self-affine model. The additions of certain proportions of silica to zirconia have resulted into a densification of the microstructure. This has also resulted into a better grain structure ordering which ultimately led to display of superior spectral refractive index profiles. Besides these films also were demonstrated superior band gap values at the same time. Such situations very distinctly displayed the violation of most popular Moss rule which establishes an inverse relationship between the refractive index and band gap. With respect to practical applications, however, these composite films have opened up a new dimension in which it is possible to extend the range of refractive index tunability in codeposition process beyond the limits of the participating components.

References

- [1] L. Armelao, C. Eisenmenger-Sittner, M. Groenewolt, S. Gross, C. Sada, U. Schubert, E. Tondello, A. Zattin, *J. Mater. Chem.* 15 (2005) 1838.
- [2] W.J. Gunning, R.L. Hall, F.J. Woodberry, W.H. Southwell, N.S. Gluck, *Appl. Opt.* 28 (1989) 2945.
- [3] M.F. Ouellette, R.V. Lang, K.L. Yan, R.W. Bertram, R.S. Owles, D. Vincent, *J. Vac. Sci. Technol. A* 9 (1991) 1188.
- [4] R. Jacobsson, Inhomogeneous and coevaporated homogeneous films for optical applications, in: G. Hass, M.H. Francombe, R.W. Hoffman (Eds.), *Physics of Thin Films*, vol. 8, Academic, New York, 1975, pp. 51–98.
- [5] H.O. Sankur, J. DeNatale, W.J. Gunning, *Appl. Opt.* 30 (1991) 497.
- [6] H. Sankur, W. Gunning, *J. Appl. Phys.* 66 (1989) 807.
- [7] S.H. Mohamed, O. Kappertz, J.M. Ngaruiya, T. Niemeier, R. Drese, R. Detemple, M.M. Wakkad, M. Wuttig, *Phys. Status Solidi (A)* 201 (2004) 90.
- [8] Y. Utsugi, *Phys. Status Solidi (B)* 212 (1999) R9.
- [9] A. Boukourt, B. Abbar, H. Abid, M. Sehil, Z. Bensaad, B. Soudini, *Mater. Chem. Phys.* 82 (2003) 911.
- [10] M.A. Salem, *Chin. J. Phys.* 41 (2003) 288.
- [11] K.L. Vodopyanov, *J. Opt. Soc. Am. B* 16 (1999) 1579.
- [12] N.M. Ravindra, V.K. Srivastava, *Infrared Phys.* 19 (1979) 605.
- [13] H. Finkenrath, *Infrared Phys.* 28 (1988) 363.
- [14] J.S. Seeley, R. Hunneman, A. Whatley, *Appl. Opt.* 20 (1981) 31.
- [15] D.J. Norris, Y.A. Vlasov, *Adv. Mater.* 13 (2001) 371.
- [16] J. Fesquet, *J. Opt. Soc. Am. A* 3 (1986) 369.
- [17] M. Kano, K. Sugiyama, *Electron. Lett.* 16 (1980) 146.

- [18] P. Gu, X. Liu, J. Tang, *Appl. Opt.* 32 (1993) 1528.
- [19] D. Reicher, K. Jungling, *Appl. Opt.* 36 (1997) 1626.
- [20] B.J. Pond, J.I. DeBar, C.K. Carniglia, T. Raj, *Appl. Opt.* 28 (1989) 2800.
- [21] E.N. Farabaugh, D.M. Sanders, *J. Vac. Sci. Technol. A* 1 (1983) 356.
- [22] A. Feldman, X. Ying, E.N. Farabaugh, *Appl. Opt.* 28 (1989) 5229.
- [23] A. Feldman, E.N. Farabaugh, W.K. Haller, D.M. Sanders, R.A. Stempniak, *J. Vac. Sci. Technol. A* 4 (1986) 2969.
- [24] W.H. Koo, S.M. Jeong, S.H. Choi, H.K. Baik, S.J. Lee, S.M. Lee, *J. Vac. Sci. Technol. A* 22 (2004) 2048.
- [25] H.N. Yang, A. Chan, G.C. Wang, *J. Appl. Phys.* 74 (1993) 101.
- [26] V.I. Trofimov, *Thin Solid Films* 428 (2003) 56.
- [27] Z.-J. Liu, N. Jiang, Y.G. Shen, Y.-W. Mai, *J. Appl. Phys.* 92 (2002) 3559.
- [28] C.H. Zhang, Z.-J. Liu, K.Y. Li, Y.G. Shen, J.B. Luo, *J. Appl. Phys.* 95 (2004) 1460.
- [29] H. Lee, I.-Y. Kim, S.-S. Han, B.-S. Bae, M.K. Choi, I.-S. Yang, *J. Appl. Phys.* 90 (2001) 813.
- [30] A.V. Osipov, F. Schmitt, P. Hess, *Thin Solid Films* 472 (2005) 31.
- [31] Y.J. Cho, N.V. Nguyen, C.A. Richter, J.R. Ehrstein, B.H. Lee, J.C. Lee, *Appl. Phys. Lett.* 80 (2002) 1249.
- [32] B. von Blanckenhagen, D. Tonova, J. Ullmann, *Appl. Opt.* 41 (2002) 3137.
- [33] S.H. Wemple, M. DiDomenico Jr., *Phys. Rev. B* 3 (1971) 1338.
- [34] S.H. Wemple, *Phys. Rev. B* 7 (1973) 3767.
- [35] M.A. Gaffar, A. Abu El-Fadl, S. Bin Anooz, *Cryst. Res. Technol.* 38 (2003) 798.
- [36] S.H. Wemple, M. DiDomenico Jr., *Phys. Rev. Lett.* 23 (1969) 1156.
- [37] H.N. Yang, A. Chan, G.C. Wang, *J. Appl. Phys.* 74 (1993) 101.
- [38] Y. Chen, W. Huang, *Meas. Sci. Technol.* 15 (2004) 2005.
- [39] Z.J. Liu, N. Jiang, Y.G. Shen, Y.W. Mai, *J. Appl. Phys.* 92 (2002) 3559.
- [40] C.H. Zhang, Z.J. Liu, K.Y. Li, Y.G. Shen, J.B. Luo, *J. Appl. Phys.* 95 (2004) 1460.
- [41] A. Mannelquist, N. Almquist, S. Fredriksson, *Appl. Phys. A* 66 (1998) S891.